

Cross-Bar SnO₂-NiO Nanofiber-Array-Based Transparent Photodetectors with High Detectivity

Zhenghao Long, Xiaojie Xu, Wei Yang, Mingxiang Hu, Dmitry V. Shtansky, Dmitri Golberg, and Xiaosheng Fang*

An cross-bar structure is employed to design a transparent *p-n* junction-based photodetector. The device consisting of aligned *n*-SnO₂ and *p*-NiO nanofibers is prepared via a mature electrospinning process that is suitable for commercial applications. It exhibits a high detectivity of 2.33×10^{13} Jones under 250 nm illumination at -5 V, outperforming most state-of-art SnO₂-based UV photodetectors. It is also endowed with a self-powered feature due to a photovoltaic effect from the *p-n* junction, resulting in a photocurrent of 10^{-10} A, responsivity of 30.29 mA W⁻¹ at 0 V bias, and detectivity of 2.24×10^{11} Jones at 0.05 V bias. Moreover, the device is highly transparent (over 90% toward visible light) due to the wide band gap of photoactive materials and well-designed cross-bar fiber structure. Additionally, an *n*-SnO₂-*p*-ZnO:Ag (Ag doped ZnO) self-powered UV photodetector is fabricated that shows good performance and give another example of the use of the cross-bar structure.

nanostructures thanks to their unique properties including high surface-to-volume ratio and anisotropic transmission characteristics, were intensively explored in the past decades.^[12–18] However, there still remain several key challenges to realize practical high-performance transparent PDs. First, most 1D UV PDs, which are synthesized through high-temperature processes, including chemical vapor deposition (CVD) and hydrothermal methods, are tangled nanowires or vertically formed nanoarrays, which can hardly reach a visible light transmittance (higher than 80%) despite the wide band gaps of active semiconductors. Second, most PDs are desired with a self-powered feature to meet the demand of low power consumption. However, it is more difficult to

1. Introduction

Transparent electronics is an important branch of the optoelectronics and related devices,^[1–10] such as touch screens, smart windows, and displays. Ultraviolet (UV) photodetectors (PDs), which convert UV light into electric signals, are the cornerstones of many optoelectronic systems.^[11] Transparent PDs, especially those based on one dimensional (1D)

realize such features in a transparent optoelectronic device, as it needs to allow most of visible light to pass through, while, at the same time, to guarantee enough light absorption to power the device.

To address these problems, we developed a novel fabric-like *p-n* junction PD with aligned *p*-NiO nanofibers interlaced by aligned *n*-SnO₂ nanofibers. A well-designed cross-bar structure, which is realized by a simple and effective electrospinning technique, not only provided the device with good transparency, but also made it possible to reach a high responsivity and high detectivity. Moreover, the PD could work in a self-powered mode due to the photovoltaic effect from the cross-bar *p-n* junctions.

SnO₂, with a wide band gap of 3.6 eV,^[19,20] high electron concentration, and high physicochemical stability, is a good *n*-type candidate for high-performance UV PDs. Most SnO₂-based PDs have shown a good responsivity with high photocurrents. However, they also have a high dark current because of their high carrier density, thus resulting in a low detectivity. By contrast, for a *p-n* junction, the built-in electric field may block the carrier paths through the interface, and the dark current can thus be greatly reduced. As a result, the detectivity can be improved, especially under a reverse bias.


In this work, an cross-bar structure was employed to fabricate transparent *p-n* junction-based photodetectors. For the *p*-type candidate, NiO, a widely studied *p*-type semiconductor in various optoelectronic devices, was selected to build a type-II heterojunction with SnO₂ for the effective charge separation.

Z. H. Long, Dr. X. J. Xu, W. Yang, M. X. Hu, Prof. X. S. Fang
Department of Materials Science
Fudan University
Shanghai 200433, P. R. China
E-mail: xshfang@fudan.edu.cn

Prof. D. V. Shtansky
National University of Science and Technology "MISIS,"
Moscow 119049, Russia

Prof. D. Golberg
Science and Engineering Faculty
Queensland University of Technology (QUT)
Brisbane, QLD 4000, Australia

Prof. D. Golberg
International Center for Materials Nanoarchitectonics (MANA)
National Institute for Materials Science (NIMS)
Tsukuba 305004, Japan

 The ORCID identification number(s) for the author(s) of this article can be found under <https://doi.org/10.1002/aem.201901048>.

DOI: 10.1002/aem.201901048

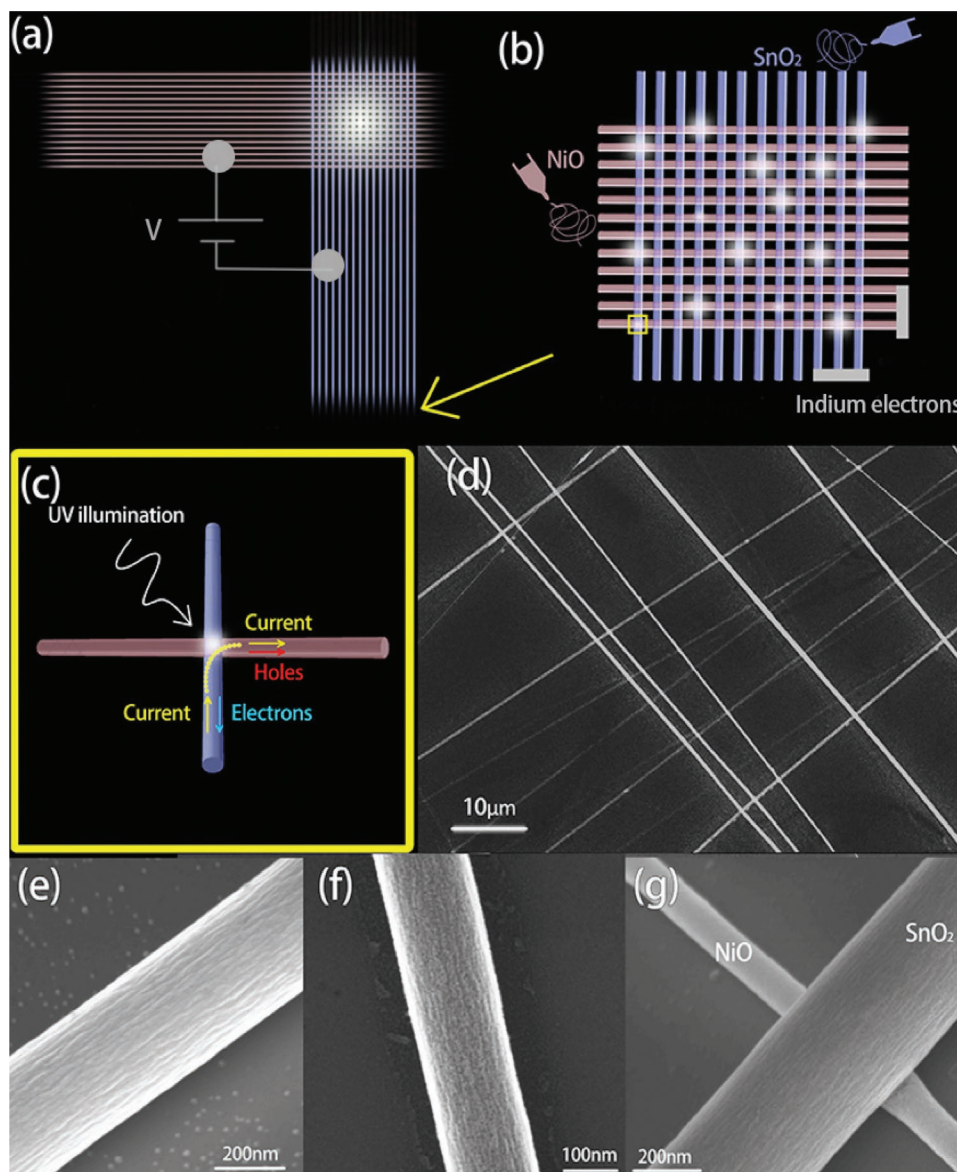


Figure 1. Structure of SnO₂-NiO heterojunction arrays; a) Schematic diagram of cross-bar *p-n* junction connected to external circuit, b) Illustration of SnO₂-NiO *p-n* junction arrays and c) working principle of this *p-n* junction. SEM images of d) SnO₂-NiO nanofiber arrays, e) SnO₂ nanofiber, f) NiO nanofiber and g) intersection point of SnO₂ and NiO nanofibers.

As a result, the dark current of SnO₂ was significantly reduced, for about 1000 times, resulting in a high detectivity of 2.33×10^{13} Jones. The SnO₂-NiO PD has a high responsivity of 8.67 A W^{-1} . The on/off rate has also been increased to 196, which is about two orders of magnitude higher than that of pure SnO₂ and NiO nanofiber PDs. SnO₂-NiO PD has also a faster response and recovery speed compared with a plain SnO₂ PD. In addition, SnO₂-NiO combination makes a self-powered PD with a photocurrent of 10^{-10} A under 250 nm illumination at 0 V bias, thanks to the photovoltaic effect of the *p-n* junction. Moreover, to demonstrate the universality of this method, Ag-doped ZnO, a previously reported *p*-type semiconductor,^[21] was also used to form a *p-n* heterojunction with SnO₂. The SnO₂-ZnO:Ag PD showed a high optoelectronic performance as well.

2. Results and Discussion

The cross-bar n-SnO₂-p-NiO photodetector and external circuit was illustrated in **Figure 1**. In our device, as shown in **Figure 1b**, highly aligned NiO nanofibers serve as the bottom layer, while the aligned SnO₂ fibers are placed on top of it, resulting in a porous cross-bar structure. Thus, both NiO and SnO₂ nanofibers may absorb photons and generate electrons and holes upon UV illumination, and then the photoinduced electron-hole pairs may be quickly and effectively separated due to the Type-II heterojunction of NiO and SnO₂, leading to a high detectivity. **Figure 1c** shows the separation of photoinduced electron-hole pairs at the junction of SnO₂ and NiO nanofibers. On the other hand, this device configuration and facile preparation method can easily be adopted in other material systems toward

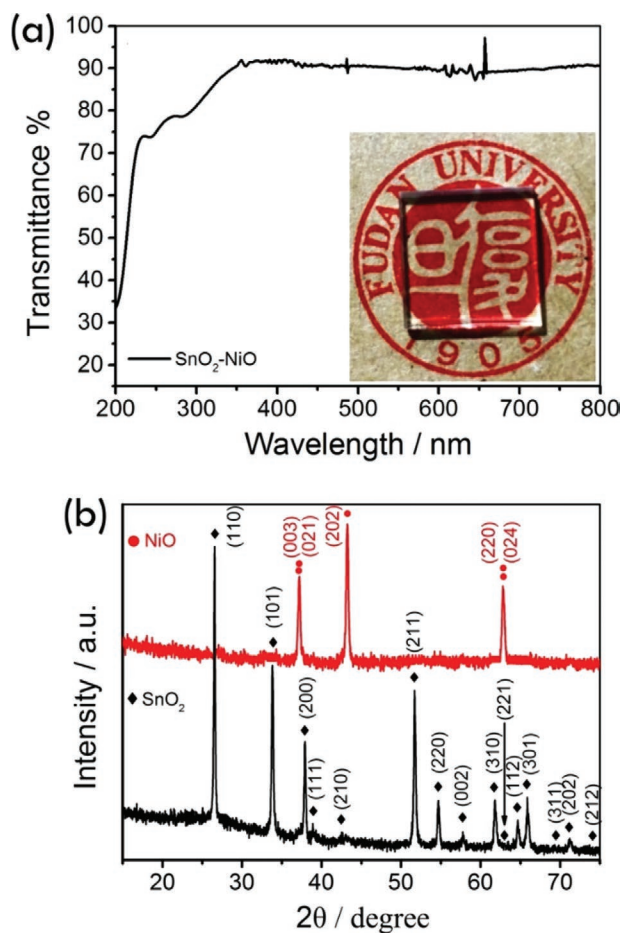


Figure 2. a) Transmittance spectra and b) XRD pattern of a SnO₂-NiO-based photodetector.

exploration of transparent optoelectronic devices, as was further exemplified by us for a case of SnO₂-ZnO:Ag PDs.

Scanning electron microscopy (SEM) images of the device are shown in Figure 1. Figure 1d depicts the cross-bar SnO₂-NiO nanofiber arrays prepared by a low-cost electrospinning method. The upper layer, in which the fibers are thicker, is the SnO₂ nanofiber array. And the fibers underneath are made of NiO. With a closer observation of the individual fibers, as shown in Figure 1e,f, the SnO₂ nanofiber has a diameter of ≈300 nm and the NiO nanofiber has a diameter of ≈150 nm. The intersection point of two kinds of nanofibers is illustrated in Figure 1g.

The transmittance of SnO₂-NiO PD is presented in Figure 2a, it has an average transmittance of ≈90% in the visible range, while showing strong absorption at a wavelength of <350 nm, which agrees well with the large band gaps of SnO₂ (3.6 eV) and NiO (3.5 eV).^[22] The high transparency is mainly attributed to the pores of the cross-bar SnO₂-NiO fiber structure and wide band gaps of the photoactive semiconductors. A photograph which further demonstrates the transparency of this device is displayed in the inset.

The crystal structures of SnO₂ and NiO nanofibers were analyzed using X-ray diffraction (XRD); the results are displayed in Figure 2b. The diffraction peaks of both SnO₂ and NiO

nanofibers match well with the anatase phase of SnO₂ (JCPDS No. #99-0024) and NiO (JCPDS No. #89-7101). Besides, the sharp peaks also indicate that both SnO₂ and NiO nanofibers have a good crystallinity.

Figure 3a shows the current density–voltage curve of nanofiber array PDs made of pure SnO₂ fibers, NiO fibers, and cross-bar SnO₂-NiO fibers under dark condition and 300 nm illumination. Compared with SnO₂ PD, the dark current of SnO₂-NiO is significantly reduced because of the low conductivity of NiO nanofiber arrays and the built-in electric field between SnO₂ and NiO arrays. The noticeable rectifying behavior apparent in the curve of SnO₂-NiO without illumination further suggests the successful formation of a *p-n* junction. The SnO₂-NiO *p-n* junction-based PD has a much higher on/off ratio of 196, which is about 70 times and 110 times respectively higher than these of plain SnO₂ and NiO nanofiber PD arrays.

To further discuss the photoresponse of the devices, the *I-t* curve under a periodic on/off switching (30 s) upon 300 nm light illumination at −5 V bias is presented in Figure 3b. Upon UV illumination, the current of SnO₂-NiO PD increases gradually and then reaches a stable value. When the light is turned off, the current decreases. In contrast, the NiO PD has a relatively faster rise speed, while a much longer decay time. In other words, once the light is off, the current of the NiO PD decreases a little and then stops decreasing. For the plain SnO₂ phase, both the response and recovery speeds are very slow. Therefore, with the formation of a *p-n* junction, the response speed, recovery speed, and on/off ratio have all been optimized.

Spectral responsivity (R_λ), which shows how efficiently a PD responds to the light, is a representative parameter to evaluate the performance of a PD. It can be calculated using the following equation:

$$R_\lambda = (I_{ph} - I_d) / PS \quad (1)$$

Where I_{ph} is the photocurrent, I_d is the dark current, P is the light power density, and S is the effective area under irradiation ($2.17 \times 10^{-5} \text{ cm}^2$, the calculation is shown in the Supporting Information). In this work, the responsivity of cross-bar SnO₂-NiO fiber array PD was taken at a wavelength of 250–400 nm at −5 V bias, as indicated in the black curve in Figure 3c. The cutting-off wavelength is 320 nm, which means there is a negligible photoresponse at wavelengths longer than 320 nm, and the highest responsivity occurs at 250 nm, approaching that of ≈8.67 AW^{−1}. Furthermore, the external quantum efficiency (EQE) was calculated to be 4337.17%, which is because the trap states in *p*-NiO trapped photogenerated holes, and the electron mobility in *n*-SnO₂ is relatively high, so that the electrons will recycle several times in the circuit and achieved a photogain effect^[23,24]

Detectivity (D^* , typically quoted in Jones) is another important parameter for PDs. It shows the ability to detect weak signals from a noisy environment. The detectivity is calculated via the following equation:

$$D^* = R_\lambda / (2eI_d / S)^{1/2} \quad (2)$$

Where R_λ is the responsivity, e is the electron charge, I_d is the dark current, and S is the effective area under irradiation. Because of the significant decrease of the dark current in

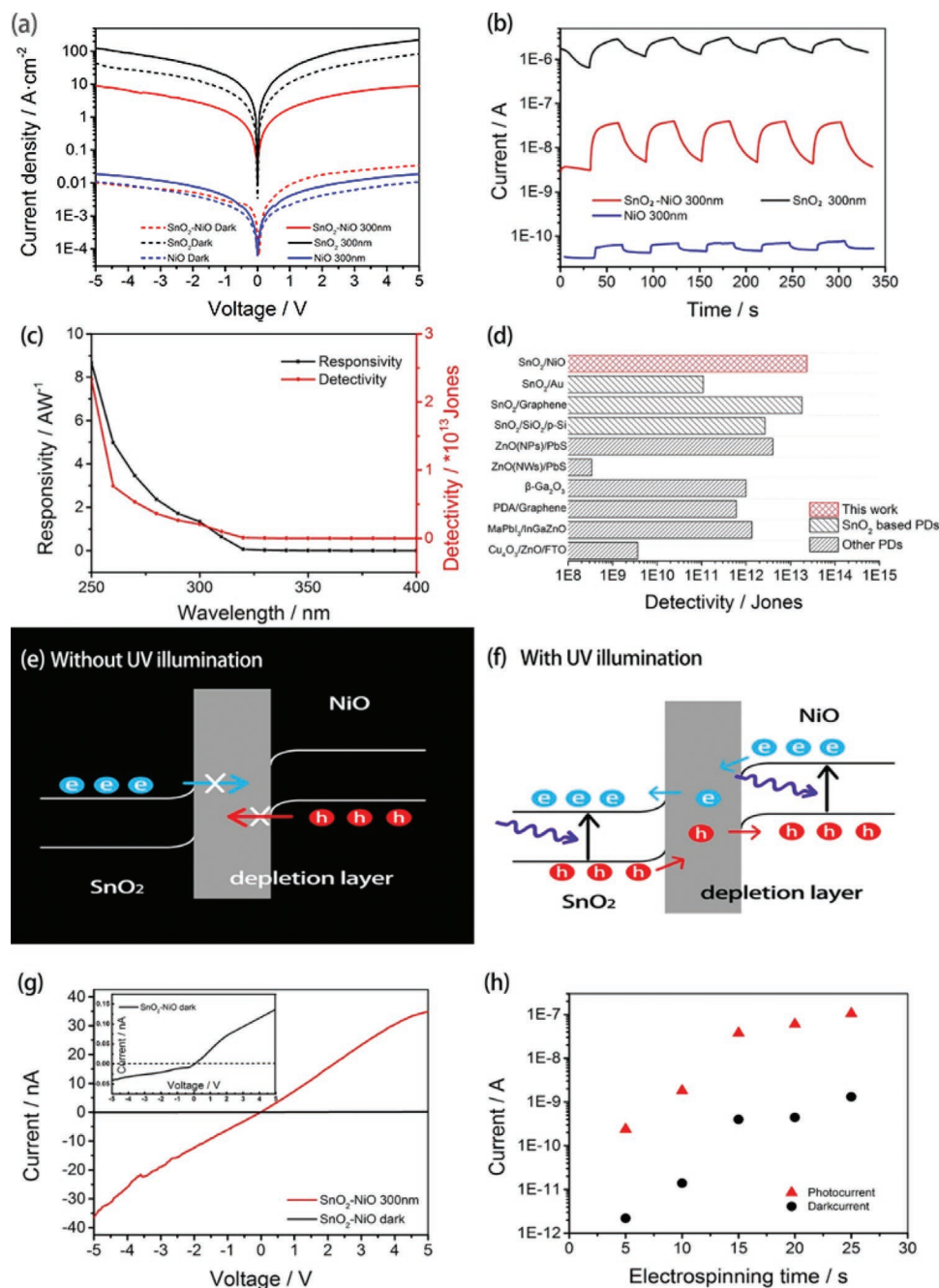


Figure 3. Logarithmic a) current density–voltage curves and b) I – t curves of pure SnO₂, NiO nanofiber arrays, and SnO₂-NiO PDs. c) Responsivity and detectivity of SnO₂-NiO PD under -5 V bias. d) Detectivity of recently reported PDs and this work. Schematic diagrams of the working principle e) without illumination and f) under UV illumination. g) Linear I – V curves of SnO₂-NiO PD with and without UV illumination. h) Photocurrent and dark current of SnO₂-NiO PDs with different density of nanofibers.

SnO₂-NiO PD, it shows a high detectivity to UV illumination at a wavelength of <320 nm. Similar to responsivity, detectivity is very low at wavelengths longer than 320 nm. As shown in red in Figure 3c, the detectivity follows the trend of responsivity and shows a maximum detectivity of 2.33×10^{13} Jones at 250 nm, which outperformed most state-of-art SnO₂-based heterojunction PDs, as summarized in Figure 3d. It suggests that the SnO₂-NiO PD has a remarkable sensitivity to weak UV illumination, which demonstrates its great potentials in

applications for low UV density conditions and related cases. To further discuss the performance of SnO₂/NiO PD, Figure 3g presents some other recently reported PDs with high detectivity.^[25–40] A more detailed summary of recent publications of PDs can be found in Table S1, Supporting Information.

Figure 3e,f illustrates the working principle of SnO₂-NiO PD. In a p - n junction, the holes, which are the dominant carriers in p -type semiconductors (P), will diffuse from P to the n -type semiconductor (N) at the interface due to the concentration

gradient, *vice versa* for electrons. As a result, a depletion layer, which hinders free carriers travels through the interface, is formed at the interface of P and N. In the dark, as shown in Figure 3e, free carriers can hardly cross the depletion layer, leading to a remarkably low current. Moreover, because of the redistribution of carriers, the P will be negatively charged and the N will be positively charged, resulting in a built-in electric field, with a direction from N to P. Under UV illumination, as shown in Figure 3f, free electrons at the conduction band (CB) of P and free holes at the valence band (VB) of N will be injected into the depletion layer, and then separated by the built-in electric field. Therefore, the device exhibits a relatively high current density under UV illumination, resulting in a high on-off ratio and a high detectivity. In addition, under the forward bias, and P being positive with respect to N, the depletion layer becomes thinner and the built-in electric field becomes weaker. On the other hand, under the reverse bias, and P becoming negative with respect to N, the depletion layer is widened and the built-in electric field is strengthened. Therefore, the current density under the forward bias will be much higher than that under reverse bias without illumination, resulting in a rectification effect. Figure 3g shows the *I-V* curve of SnO₂-NiO PD with and without 300 nm illumination. The current density under -5 V bias is significantly lower than that under 5 V bias. A rectification effect can be seen in the zoomed-in curve of dark current, which shows a rectification ratio of 3.45. Under UV illumination, photocarriers are continuously generated and injected into the depletion layer, thus the rectification effect can hardly be noticed.

In addition, the effective area is also an important factor which affects both photocurrent and dark currents. In the electrospinning process, the spinning time is positively correlated to the surface area. The relationship between electrospinning time and current density under dark and 300 nm illumination is illustrated in Figure 3h. As the electrospinning time increases, both dark current and photocurrent increase. However, the on/off ratio of these devices ($\approx 10^2$) has no big difference (as the relationship between electrospinning time and density of nanofibers is not linear, the current densities have not shown a linear correlation with dark and photocurrent density). Thus, our device can be easily adjusted in terms of the current density without changing the on/off rate, suggesting its potentials to be applied in versatile environments. The corresponding optical microscope image of each device is shown in Figure S1, Supporting Information.

A self-powered PD can be fabricated based on the photovoltaic effect from *p-n* junctions. Under 0 V bias, the built-in electric field from N to P leads to a dark current from N to P. Once the device is exposed to illumination, photoinduced electron-hole pairs become separated by the built-in electric field, leading to a photocurrent much higher than the dark current without any external bias. Based on this phenomenon, a *p-n* junction-based photodetector may work even at 0 V, relieving a photodetector from external power sources. Figure 4 shows the self-powered feature of the device. Figure 4a displays a zoomed-in *I-V* curve of SnO₂-NiO with and without 250 nm illumination. Under 0 V bias, photocurrent reaches 10⁻¹⁰ A and the on/off ratio becomes about 140. Besides, minority carriers of each material are pushed through the depletion

zone to the junction. This action causes a very small leakage current to occur, which cause *I-V* curve under dark dose not cross the origin. Generally, leakage current is so small that it can be considered as negligible. Figure 4b shows the *I-t* curve under 60 s periodic switching of 250 nm light. Upon illumination, the current density gradually increases to about 10⁻¹⁰ A in 8 s. When the illumination is off, the current density gradually decreases until the illumination is turned on again. Several cycles of on-off switching test were carried out and the performance of the device was found to remain nearly unchanged, demonstrating its good stability. The responsivity and the detectivity of this device under 0 V bias were also calculated, with

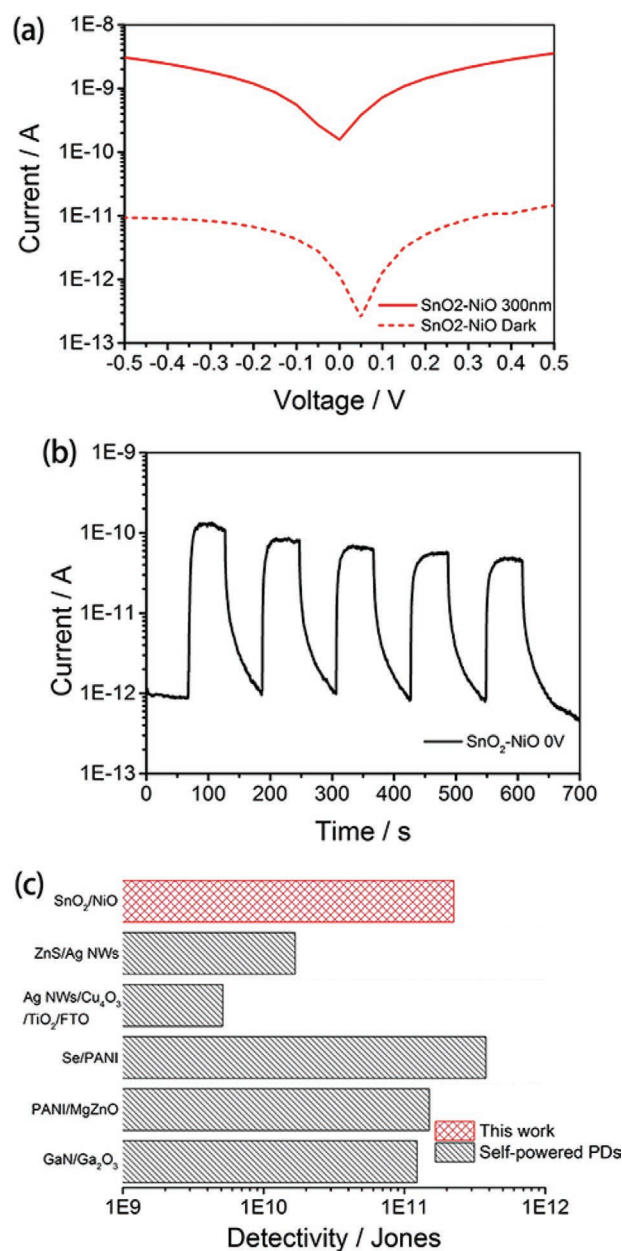


Figure 4. a) *I-V* curves of SnO₂-NiO with and without UV illumination under external bias near 0 V. b) *I-t* curve of SnO₂-NiO under 0 V bias. c) Detectivity under 0 V of recently reported PDs compared to this work.

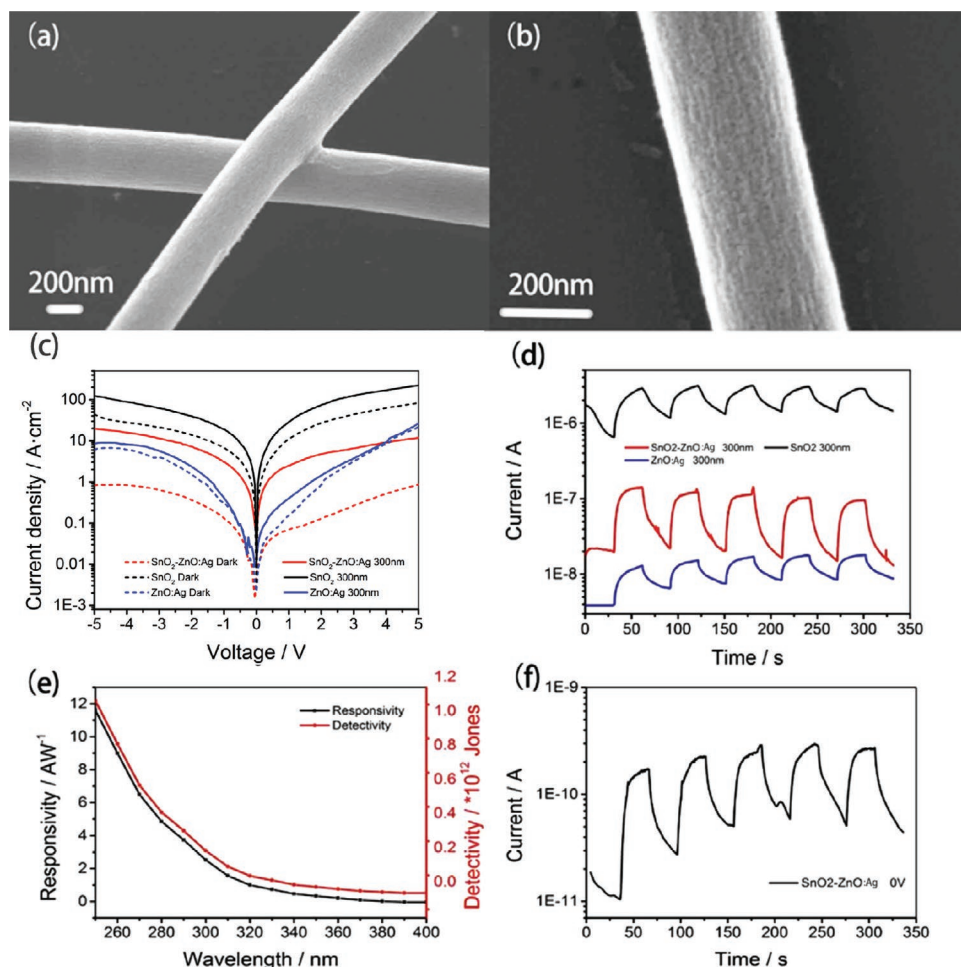


Figure 5. SEM images of a) $\text{SnO}_2\text{-ZnO:Ag}$ heterojunction and b) ZnO:Ag nanofiber. Logarithmic c) current density–voltage curves and d) I – t curves of pure SnO_2 , ZnO:Ag nanofiber arrays, and $\text{SnO}_2\text{-ZnO:Ag}$ PDs. e) Responsivity and detectivity of $\text{SnO}_2\text{-ZnO:Ag}$ PD, f) I – t curves of $\text{SnO}_2\text{-ZnO:Ag}$ PD under 0 V bias.

a maximum responsivity of 30.29 mA W^{-1} . Moreover, thanks to the present device configuration, which is particularly able to detect weak signals, the device has a high detectivity of 2.24×10^{11} Jones under a small external voltage (0.05 V bias). Figure 4c illustrates the comparison of the detectivity under 0.05 V low voltage (or 0 V bias in some papers) with the state-of-art self-powered PDs. As there are only very limited reports on self-powered high-performance SnO_2 -based PDs, the performance of this $\text{SnO}_2\text{-NiO}$ PD is compared with other self-powered PDs.^[41–47] For more details, see Table S2, Supporting Information.

To demonstrate the effectiveness and generality of the present device design and the employed preparation method for making transparent optoelectronic devices, aligned Ag-doped ZnO nanofibers were chosen as a p -type semiconductor to replace NiO . As shown in Figure 5a, the SnO_2 nanofiber is placed on a Ag-doped ZnO nanofiber (ZnO:Ag nanofiber). The active junction is small, leaving the rest of the fibers exposed to the illumination. Morphological details of the Ag-doped ZnO nanofiber can be found in Figure 5b, the diameter of ZnO:Ag nanofiber is about 320 nm, which is much thicker than that of the NiO nanofiber, and close to that of SnO_2 nanofiber. Like

NiO , ZnO:Ag will also form a Type II band structure with SnO_2 . Even though ZnO is an n -type semiconductor, with Ag doping, the Fermi energy is moved downward, resulting in a higher hole concentration and transformation to the p -type material.^[21] The concentration gradient of electrons and holes between SnO_2 and ZnO:Ag results in a depletion layer at the interface; as a result, the $\text{SnO}_2\text{-ZnO:Ag}$ heterojunction works based on the same principle as that of the $\text{SnO}_2\text{-NiO}$ p - n junction. Current density–voltage curves are displayed in Figure 5c. Because of the depletion layer, the on/off ratio has been improved, about 8 and 17 times higher than that of the SnO_2 and ZnO:Ag nanofiber arrays, respectively. I – t curves in Figure 5d suggest that the response and recovery speeds have also been increased with the formation of the p - n junction. The responsivity and detectivity curves are shown in Figure 5e; the $\text{SnO}_2\text{-ZnO:Ag}$ PD delivers the highest responsivity of 11.61 A W^{-1} and the highest detectivity of 1.12×10^{12} Jones under 250 nm illumination. The detectivity is also higher than for many SnO_2 -based PDs. Moreover, as the p - n junction-based PD, the device also has a self-powered feature with a photocurrent higher than 0.1 nA under 300 nm illumination even at 0 V bias. The I – t curve under 0 V bias is shown in Figure 5f. In addition, the

cross-bar ZnO:Ag and SnO₂ nanofibers-based PD is also highly transparent (see details in Supporting Information).

3. Conclusion

In summary, textile-like cross-bar *p-n* junction photodetectors made of *n*-SnO₂ and *p*-NiO nanofibers have been fabricated through a simple electrospinning method. The device shows a high transparency (of >90% transmittance at the visible range) owing to the large band gaps of the constituting materials and cross-bar fiber array configuration. Such cross-bar *p-n* junction not only has a large surface area under illumination, but also helps to decrease the dark current due to the creation of the depletion region, thus reducing the noise level. As a result, the device is endowed with an excellent weak signal detection ability. For example, the transparent *n*-SnO₂/*p*-NiO PD has a high detectivity of 2.33×10^{13} Jones under 250 nm illumination at -5 V, which is higher than most of the SnO₂-based PDs. Moreover, the device even delivers high detectivity of 2.24×10^{11} Jones and responsivity of 30.29 mA W^{-1} under 250 nm illumination at 0.05 and 0 V biases, respectively, due to the photovoltaic effect, which outperforms most of the state-of-art self-powered PDs.

The last but not least, as the device architecture and preparation method are compatible with the mature textile technology, the regarded technique can easily be adopted for designing other transparent optoelectronic components, which is well exemplified by the creation of the cross-bar *n*-SnO₂/*p*-ZnO:Ag fiber array PD. This device also shows an improved on/off ratio, response and recovery speeds, a high detectivity, and a self-powered feature, suggesting that our work presents a facile, effective, and general way to develop next-generation transparent electronic devices.

4. Experimental Section

All the chemicals were purchased from Sinopharma company and used without further purification.

Preparation of Aligned Nanofiber Arrays with Sn²⁺: First, 0.6 g of SnCl₂·2H₂O powder was dissolved in 2.0 g ethanol to obtain a clear solution A. And 0.4 g of polyvinylpyrrolidone ($M = 1\,300\,000 \text{ g mol}^{-1}$) was dissolved in 2.2 g of *N,N*-dimethylformamide to obtain a clear solution B. Solution A was mixed with solution B and the mixture was vigorously stirred overnight. The mixture became clean and was squeezed into the needle of a syringe at a feeding rate of 1 mL h^{-1} . The collectors were made of two pieces of aluminum foil, which were placed in parallel with about 5 cm gap. The needle and the collectors were connected with 10 and -3 kV power supplies, respectively. The distance between the needle and the collector was 15 cm. A 1×1 cm square quartz substrate, of which half was covered by a paper, was put within the gap of the collectors. The electrospun nanofibers form an array across the gap and cover the other half of the substrate. Then, we used a blade to cut off those nanofibers out of the substrate.

Fabrication of Cross-Bar SnO₂-NiO Nanofiber Arrays-Based PD: Similar to the fabrication of nanofiber arrays with Sn²⁺, 0.4 g Ni(NO₃)₂·6H₂O was dissolved into 1 g deionized water to form solution A. And solution B was a mixture of 0.3 g polyvinylpyrrolidone ($M = 1\,300\,000 \text{ g mol}^{-1}$) and 3 g ethanol. Solution A was mixed with solution B and the mixture was vigorously stirred overnight. The electrospun process was the same as during the preparation of nanofiber arrays with Sn²⁺, by covering half of the substrate, on which there were nanofiber arrays with Sn²⁺; the

nanofiber arrays with Ni⁺ were prepared in a perpendicular direction. After that, the device was placed in an oven heated to 60 °C to fully remove the solvent. Then, the device was annealed in air at 550 °C for 2 h at a heating rate of 1 °C min^{-1} , and the oxidized inorganic nanofiber arrays on the quartz substrate were obtained. Finally, two small indium dots were pressed on SnO₂ and NiO nanofiber arrays as the contacts.

Fabrication of Cross-Bar SnO₂-ZnO:Ag Nanofiber Arrays-Based PD: Similar to the fabrication of SnO₂-NiO PD, the solution A was made of 0.4 g Zn(NO₃)₂·6H₂O, 0.0229 g AgNO₃ and 1 g deionized water. The solution B was made of 0.45 g polyvinylpyrrolidone ($M = 1\,300\,000 \text{ g mol}^{-1}$) and 3 g ethanol. Solutions A and B were mixed and vigorously stirred overnight. The electrospinning and post-annealing processes were the same as those during the fabrication of SnO₂-NiO PD. Indium was also used for the contacts.

Characterizations: SEM images were taken by means of a field-emitting scanning electron microscope (Zeiss Sigma). The phases were identified by X-ray diffraction (Bruker D8-A25) using Cu K α radiation ($\lambda = 0.15406 \text{ nm}$) with 2θ ranging from 15° to 75° . Optical transmittance spectra of samples were acquired on an Aflent 8453 UV-Vis spectrophotometer. The optoelectronic properties were recorded with a semiconductor characterization system (Keithley 4200-SCS). The light source was a Xenon arc lamp with a monochromator.

Supporting Information

Supporting Information is available from the Wiley Online Library or from the author.

Acknowledgements

Z.L. and X.X. contributed equally to this work. The authors appreciate Jiaxin Chen and Dr. Yong Zhang for their kind help to this work. This work was supported by the National Key Research and Development Program of China (Grant No. 2017YFA0204600), the National Natural Science Foundation of China (11811530065), the Science and Technology Commission of Shanghai Municipality (18520710800), FDUROP (Fudan's Undergraduate Research Opportunities Program) (Grant No.17421), and the Ministry of Education Joint Fund for Equipment Pre-Research (No. 6141A02033241). Part of the research was carried out in Fudan Nanofabrication Laboratory. D.G. acknowledges the Australian Research Council (ARC) Laureate Fellowship FL160100089. D.V.S. and D.G. gratefully acknowledge the financial support from the Russian Foundation for Basic Research (Agreement 18-58-53034/19).

Conflict of Interest

The authors declare no conflict of interest.

Keywords

p-n junctions, self-powered photodetectors, transparent electronics

Received: September 26, 2019

Revised: October 27, 2019

Published online: November 22, 2019

- [1] X. Q. Liu, X. Liu, J. Wang, C. Liao, X. Xiao, S. Guo, C. Jiang, Z. Y. Fan, T. Wang, X. Chen, W. Lu, W. D. Hu, L. Liao, *Adv. Mater.* **2014**, *26*, 7399.

- [2] S. Cai, X. J. Xu, W. Yang, J. X. Chen, X. S. Fang, *Adv. Mater.* **2019**, *31*, 1808183.
- [3] U. Khan, T.-H. Kim, H. Ryu, W. Seung, S.-W. Kim, *Adv. Mater.* **2017**, *29*, 1603544.
- [4] F. Wu, H. Xia, H. D. Sun, J. W. Zhang, F. Gong, Z. Wang, L. Chen, P. Wang, M. Long, X. Wu, J. Wang, W. Ren, X. Chen, W. Lu, W. Hu, *Adv. Funct. Mater.* **2019**, *29*, 1900314.
- [5] A. W. Lang, Y. Li, M. De Keersmaecker, D. E. Shen, A. M. Österholm, L. Berglund, J. R. Reynolds, *ChemSusChem* **2018**, *11*, 854.
- [6] M. Shrestha, A. Asundi, G.-K. Lau, *ACS Photonics* **2018**, *5*, 3255.
- [7] S. Lin, X. Bai, H. Wang, H. Wang, J. Song, K. Huang, C. Wang, N. Wang, B. Li, M. Lei, H. Wu, *Adv. Mater.* **2017**, *29*, 1703238.
- [8] M. K. Choi, J. Yang, D. C. Kim, Z. Dai, J. Kim, H. Seung, V. S. Kale, S. J. Sung, C. R. Park, N. Lu, T. Hyeon, D.-H. Kim, *Adv. Mater.* **2018**, *30*, 1703279.
- [9] X. L. Chen, S. H. Nie, W. R. Guo, F. Fei, W. M. Su, W. B. Gu, Z. Cui, *Adv. Electron. Mater.* **2019**, *5*, 1800991.
- [10] F. Wu, Q. Li, P. Wang, H. Xia, Z. Wang, Y. Wang, M. Luo, L. Chen, F. Chen, J. Miao, X. Chen, W. Lu, C. Shan, A. Pan, X. Wu, W. Ren, D. Jariwala, W. Hu, *Nat. Commun.* **2019**, *10*, 4663.
- [11] L. Peng, L. F. Hu, X. S. Fang, *Adv. Mater.* **2013**, *25*, 5321.
- [12] J. Xu, W. Yang, H. Chen, L. Zheng, M. Hu, Y. Li, X. S. Fang, *J. Mater. Chem. C* **2018**, *6*, 3334.
- [13] X. J. Xu, S. Shukla, Y. Liu, B. Yue, J. Bullock, L. Su, Y. Li, A. Javey, X. S. Fang, J. W. Ager, *Phys. Status Solidi RRL* **2018**, *12*, 1700381.
- [14] M. Peng, Z. Wen, M. Shao, X. Sun, *J. Mater. Chem. C* **2017**, *5*, 7521.
- [15] H. Xu, X. Han, X. Dai, W. Liu, J. Wu, J. Zhu, D. Kim, G. Zou, K. A. Sablon, A. Sergeev, Z. Guo, H. Liu, *Adv. Mater.* **2018**, *30*, 1706561.
- [16] S. Pyo, W. Kim, H.-I. Jung, J. Choi, J. Kim, *Small* **2017**, *13*, 1700918.
- [17] M. Shahid, J. Cheng, T. Li, M. A. Khan, Y. Wang, Y. Hu, M. Zhang, J. Yang, H. S. Aziz, C. Wan, H. Nishijima, W. Pan, *J. Mater. Chem. C* **2018**, *6*, 6510.
- [18] Z. M. Zhang, Y. Ning, X. S. Fang, *J. Mater. Chem. C* **2019**, *7*, 223.
- [19] T. Zhai, X. S. Fang, M. Liao, X. Xu, H. Zeng, B. Yoshio, D. Golberg, *Sensors* **2009**, *9*, 6504.
- [20] Y. Zhang, W. Xu, X. Xu, J. Cai, W. Yang, X. S. Fang, *J. Phys. Chem. Lett.* **2019**, *10*, 836.
- [21] Y. Ning, Z. Zhang, F. Teng, X. S. Fang, *Small* **2018**, *14*, 1703754.
- [22] L. X. Zheng, F. Teng, Z. Zhang, B. Zhao, X. S. Fang, *J. Mater. Chem. C* **2016**, *4*, 10032.
- [23] Y. Zhang, C. P. Chuu, J. K. Huang, C. H. Chen, M. L. Tsai, Y. H. Chang, C. Te Liang, Y. Z. Chen, Y. L. Chueh, J. H. He, M. Y. Chou, L. J. Li, *Sci. Rep.* **2015**, *4*, 3826.
- [24] Q. Zhao, W. Wang, F. Carrascoso-Plana, W. Jie, T. Wang, A. Castellanos-Gomez, R. Frisenda, *Mater. Horiz.* **2019**, <https://doi.org/10.1039/C9MH01020C>
- [25] L. Liu, C. Yang, A. Patané, Z. Yu, F. Yan, K. Wang, H. Lu, J. Li, L. Zhao, *Nanoscale* **2017**, *9*, 8142.
- [26] W. X. Ouyang, F. Teng, X. S. Fang, *Adv. Funct. Mater.* **2018**, *28*, 1707178.
- [27] S. Abbas, M. Kumar, D. Kim, J. Kim, *Small* **2019**, *15*, 1804346.
- [28] X. Xu, L. Yan, T. Zou, R. Qiu, C. Liu, Q. Dai, J. Chen, S. Zhang, H. Zhou, *ACS Appl. Mater. Interfaces* **2018**, *10*, 44144.
- [29] S. Oh, C.-K. Kim, J. Kim, *ACS Photonics* **2018**, *5*, 1123.
- [30] Z. Zheng, L. Gan, J. Zhang, F. Zhuge, T. Zhai, *Adv. Sci.* **2017**, *4*, 1600316.
- [31] P. Chetri, J. C. Dhar, *Appl. Phys. A* **2019**, *125*, 286.
- [32] J. Cai, X. Xu, L. Su, W. Yang, H. Chen, Y. Zhang, X. S. Fang, *Adv. Opt. Mater.* **2018**, *6*, 1800213.
- [33] M. Peng, Y. Wang, Q. Shen, X. Xie, H. Zheng, W. Ma, Z. Wen, X. Sun, *Sci. China Mater.* **2019**, *62*, 225.
- [34] C. Liu, A. Piyadasa, M. Piech, S. Dardona, Z. Ren, P.-X. Gao, *J. Mater. Chem. C* **2016**, *4*, 6176.
- [35] H. Choi, S. Seo, J.-H. Lee, S.-H. Hong, J. Song, S. Kim, S.-Y. Yim, K. Lee, S.-J. Park, S. Lee, *J. Mater. Chem. C* **2018**, *6*, 6014.
- [36] C. Ling, T. Guo, W. Lu, Y. Xiong, L. Zhu, Q. Xue, *Nanoscale* **2017**, *9*, 8848.
- [37] Z. Zheng, J. Yao, L. Zhu, W. Jiang, B. Wang, G. Yang, J. Li, *Mater. Horiz.* **2018**, *5*, 727.
- [38] Y. Wang, D. Yang, X. Zhou, S. M. Alshehri, T. Ahamad, A. Vadim, D. Ma, *Org. Electron.* **2017**, *42*, 203.
- [39] H. Tetsuka, *Sci. Rep.* **2017**, *7*, 5544.
- [40] Q.-M. Wang, Z.-Y. Yang, *Carbon* **2018**, *138*, 90.
- [41] P. P. Yu, K. Hu, H. Chen, L. Zheng, X. S. Fang, *Adv. Funct. Mater.* **2017**, *27*, 1703166.
- [42] S. Abbas, M. Kumar, H.-S. Kim, J. Kim, J.-H. Lee, *ACS Appl. Mater. Interfaces* **2018**, *10*, 14292.
- [43] B. Zhao, F. Wang, H. Chen, L. Zheng, L. Su, D. Zhao, X. S. Fang, *Adv. Funct. Mater.* **2017**, *27*, 1700264.
- [44] H. Y. Chen, P. Yu, Z. Zhang, F. Teng, L. Zheng, K. Hu, X. S. Fang, *Small* **2016**, *12*, 5809.
- [45] R. Zhuo, Y. Wang, D. Wu, Z. Lou, Z. Shi, T. Xu, J. Xu, Y. Tian, X. Li, *J. Mater. Chem. C* **2018**, *6*, 299.
- [46] P. Li, H. Shi, K. Chen, D. Guo, W. Cui, Y. Zhi, S. Wang, Z. Wu, Z. Chen, W. Tang, *J. Mater. Chem. C* **2017**, *5*, 10562.
- [47] Q. An, X. Meng, K. Xiong, Y. Qiu, *Sci. Rep.* **2017**, *7*, 4885.